COMPARISON AMONG THE ATMOSPHERIC BOUNDARY LAYER HEIGHT ESTIMATED FROM THREE DIFFERENT TRACERS

Gregori de Arruda Moreira[1,2,3,4*], Fábio Juliano da Silva Lopes[3], Juan Luis Guerrero-Rascado[2], Pablo Ortiz-Amezcua[2] , Alberto Cazorla[2] , Amauri Pereira de Oliveira[1], Eduardo Landulfo[3], Lucas Alados-Arboledas[2]

[1]*Institute of Astronomy, Geophysics and Atmospheric Science, São Paulo, Brazil*
[2]*Andalusian Institute for Earth System Research (IISTA-CEAMA), Granada, Spain*
[3]*Institute of Energetic and Nuclear Research (IPEN), São Paulo, Brazil*
[4]*Federal Institute of São Paulo (IFSP), São Paulo, Brazil*

**Email: gregori.moreira@usp.br*

ABSTRACT

The Atmospheric Boundary Layer (ABL) is the lowermost part of the troposphere. In this work, we analysed the combination of ABL height estimated continuously by three different remote sensing systems: a ceilometer, a Doppler lidar and a passive Microwave Radiometer, during a summer campaign, which was held in Granada from June to August 2016. This study demonstrates as the combined utilization of remote sensing systems, based on different tracers, can provide detailed information about the height of ABL and their sublayers.

1. INTRODUCTION

The lowermost region in the troposphere is denominated Atmospheric Boundary Layer (ABL). This layer "*is directly influenced by the presence of the Earth's surface, and responds to surface forcings with a time scale of about an hour or less*" (Stull, 1988), so that this process originates an unstable layer denominated Convective Boundary Layer (CBL). Close to sunset, the reduction of incidence of solar radiation causes gradual suppression of the convective processes, resulting in a weak and sporadic turbulence. Due to this phenomenon, the CBL becomes two different layers: the Stable Boundary Layer (SBL), and the Residual Layer (RL).

The height of ABL ($ABLH$) is an important parameter for several research fields, like air quality, weather forecasting, etc. The $ABLH$ can be estimated from some atmospheric variables, e.g. vertical wind speed (w), potential temperature (θ), humidity (q) and vertical aerosol distribution, which does not necessarily provide the same results due to different $ABLH$ definitions adopted by each methodology. In this paper, we propose to estimate the $ABLH$ from three different remote sensing systems: microwave radiometer (MWR), ceilometer and Doppler lidar, which can provide an $ABLH$ estimation from the respective tracers: θ, vertical aerosol distribution and w, so that the combination of these different results can provide a detailed observation of ABL and their sublayers. The data acquire campaign was held in IISTA-CEAMA (Andalusian Institute for Earth System Research - Granada [37.16◦N, 3.61◦W, 680 m a.s.l.] - Spain) from June to August 2016.

2. INSTRUMENTATION AND METHODOLOGY

2.1 The MWR Method

The ground-based passive microwave radiometer (RPG-HATPRO G2, Radiometer Physics GmbH) is situated at IISTA-CEAMA and it is part of the MWRnet - (Rose et al., 2005). It measures the sky brightness temperature with a radiometric resolution between 0.3 and 0.4 K root mean square error at 1 s integration time and uses direct detection receivers within two bands: 22-31 GHz (water vapor - K band) and 51-58 GHz (oxygen - V band), which are used for deriving relative humidity and temperature profiles, respectively. The generated profiles have a range resolution varying between 10 and 200 m in the first 2 km and varying between 200 and 1000 km up to 10km (Navas-Guzmán et al., 2014). The algorithm applied to the MWR combines two methodologies

that are the parcel method - $[PM]$ (Holzworth, 1964) and the temperature gradient method $[TGM]$ - (Stull, 1988), in order to estimate the $ABLH_{MWR}$ in convective (CBL) and stable (SBL) situations, respectively. First of all the potential temperature profile, $\theta(z)$, is derived from the temperature $(T(z))$ profile provided by the MWR, using the following equation:

$$\theta(z) = T(z) + 0.0098 * z \quad (1) \text{ (Stull, 2011)}$$

where z is the height above the sea level, and 0.0098K/m is the dry adiabatic temperature gradient. The surface potential temperature $[\theta(z_0)]$ is obtained from the meteorological station co-located with the MWR. This $\theta(z)$ profile is analyzed in order to label the situation as stable or unstable. Such analysis is made by comparing the surface potential temperature $(\theta(z_0))$ with all points in the $\theta(z)$ profile below 5 km. If all points presents $\theta(z)$ values larger than $\theta(z_0)$ the situation is considered stable and TGM is applied, otherwise the situation is assumed as unstable and the PM is used instead (Figure 1).

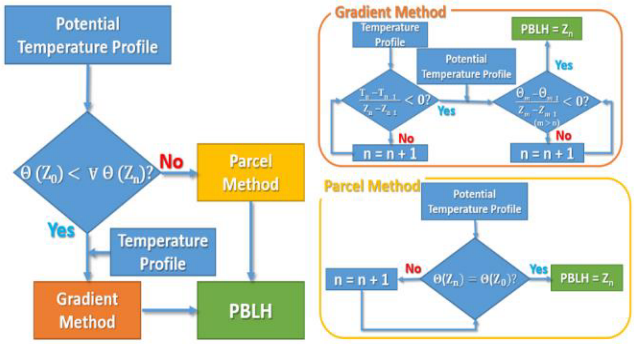

Figure 1 – Combination of two methods to estimate the $ABLH$ based on Temperature Profile.

2.2 Doppler lidar: Variance threshold method

The coherent Doppler Lidar (Halo Photonics) model Stream Line is allocated at IISTA-CEAMA. This system uses heterodyne detection to measure the Doppler shift of backscattered light. It operates an eye-safe laser transmitter vertically pointing to zenith emitting at 1.5 µm with pulse energy and repetition rate of 100 µJ and 15 KHz, respectively. The system operates with 300 gates, where the range gate length is 30 m and its first gate is located at 60 m. The data acquisition is performed in Stare mode (only the vertical wind speed is measured) with a time resolution of 2 s.

The variance of vertical wind speed $({\sigma_w}^2)$ is used to estimate the vertical size of plumes growing due to homogeneous turbulent movement. Therefore, this variable is applied as an indicator of mixing layer height $(ABLH_{Doppler})$.The $ABLH_{Doppler}$ is adopted as the first height where ${\sigma_w}^2$ has a value lower than a predetermined threshold (th_{var}), which in this paper was adopted as 0.16 m²/s² (Moreira, 2018). The σ_w^2 is calculated using time intervals of 30 minutes.

2.3 Ceilometer: Gradient method

The ceilometer Jenopitk model CHM15k is operated at the IISTA-CEAMA station. It operates with a pulsed Nd:YAG laser emitting at 1064 nm and a telescope with a field of view of 0.45 mrad. The energy per pulse is 8.4 µJ with a repetition frequency in the range of 5–7 kHz. The laser beam divergence is less than 0.3 mrad. The spatial and temporal resolution used are 15 m and 15 s, respectively.

From ceilometer data the $ABLH$ is estimated by the aerosol backscatter using the gradient method $[GM]$ (Caicedo et al., 2017). This method consists in detecting the minimum of gradient in the $RCS(z)$. Due to a typical reduction of aerosol concentration in the free troposphere (FT) when compared to ABL, this transition region (corresponding to $ABLH_{ceilometer}$) is characterized by an abrupt reduction in Range Corrected Signal ($RCS(z)$ signal).

$$ABLH_{ceilometer} = \min\left(\frac{dRCS(z)}{dz}\right) \quad (2)$$

3. RESULTS

The figure 2 presents a box whisker plot of $ABLH_{ceilometer}$. From 01:00 to 08:00 UTC, the data present low variability and a median quite constant (1000 m). At 09:00 UTC the $ABLH_{ceilometer}$ begins to present greater variability and higher average values. The highest values are observed at 15:00 UTC, so that in this period, 75% of values are higher than 1800 m. After this period, the variability of data is reduced and the median value begins to decrease reaching around 1000 m at 00:00 UTC.

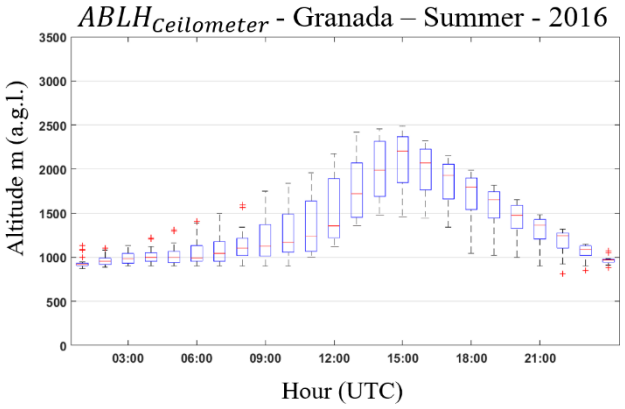

Figure 2 – Daily $ABLH_{Ceilometer}$ cycle for Summer 2016. Whiskers and boxes indicate 10, 25, 75 and 90% percentiles. The red lines represent the median.

In figure 3 a box whisker plot of $ABLH_{MWR}$ is presented. From 01:00 to 06:00 UTC the distribution presents low variability and a quite constant value of median (200 m). At 07:00 UTC the variability and the median begin to increase, reaching the maximum at 15:00 UTC (approximately 1600 m). Although the median begins to decrease at 17:00 UTC the high variability is maintained until 19:00 UTC, so that after this period the $ABLH_{MWR}$ decreases maintaining the same pattern observed during the dawn.

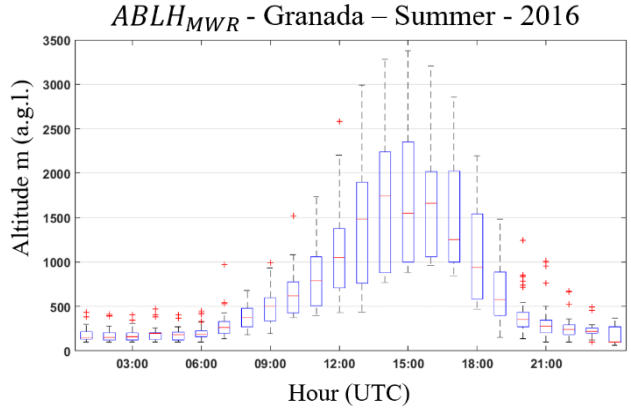

Figure 3 – Daily $ABLH_{MWR}$ cycle for Summer 2016. Whiskers and boxes indicate 10, 25, 75 and 90% percentiles. The red lines represent the median.

In figure 4 is presented a box whisker plot of the $ABLH_{Doppler}$. From 01:00 to 05:00 UTC the distribution presents low variability and a quite constant value of median (200 m). At 06:00 UTC the median value begins to increase, reaching its maximum at 15:00 UTC (1300 m) and maintaining it until 16:00 UTC. However, it is not observed an increase of the variability of distribution, as demonstrated in figures 3 and 4. At 17:00 UTC the median begins to decrease reaching at 00:00 UTC the same value observed during the dawn.

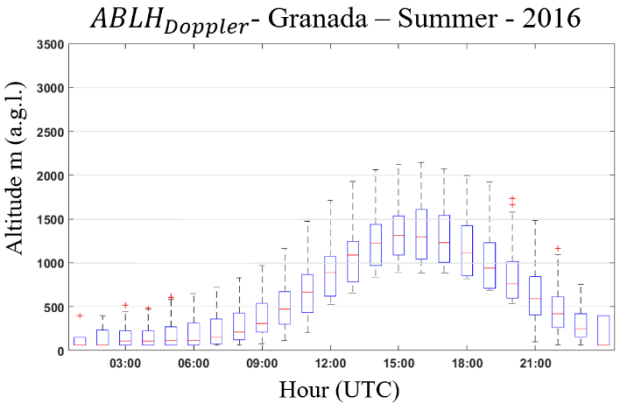

Figure 4 – Daily $ABLH_{Doppler}$ cycle for Summer 2016. Whiskers and boxes indicate 10, 25, 75 and 90% percentiles. The red lines represent the median.

The distribution of $ABLH_{Ceilometer}$ presents distinct behavior in comparison with $ABLH_{MWR}$ and $ABLH_{Doppler}$, due to the different ABL definition adopted by GM in comparison with the another ones, resulting in detection of distinct ABL sublayers.

The $ABLH_{Ceilometer}$ is based on vertical aerosol concentration, therefore it represents the full-developed CBL (often in the central region of the day) and the RL in the rest of the time. It justifies the higher values and low variability observed during the stable period.

On the other hand, $ABLH_{MWR}$ and $ABLH_{Doppler}$, although based on utilization of different tracers, have similar behavior estimating the height of CBL and SBL in convective and stable cases, respectively. It justifies the low values of median observed during the stable periods, as well as, the fast variations observed at 07:00 and 16:00 UTC. During the convective situations, $ABLH_{MWR}$ and $ABLH_{Doppler}$ have a similar behavior, although the $ABLH_{Doppler}$ has low variability in comparison with $ABLH_{MWR}$. It probably is caused by a reduction in the vertical resolution of MWR above 2000 m.

Considering the observation of different sublayers that compound the ABL, the joint observation of three $ABLH$ presented in previous figures can

provide a detailed analysis of $ABLH$ behavior, as demonstrated in figure 5, where the green, red and blue line represents the average value of $ABLH_{Ceilometer}$, $ABLH_{MWR}$ and $ABLH_{Doppler}$, respectively.

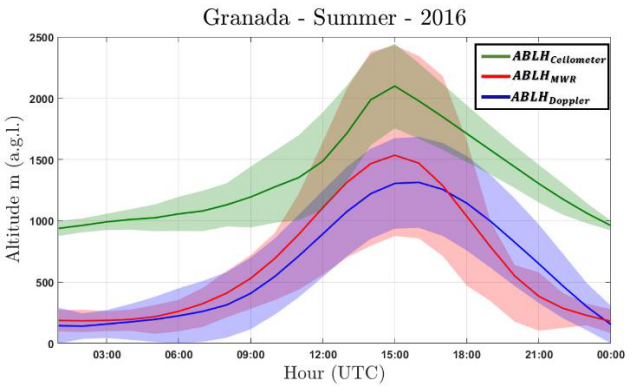

Figure 5 – Average values of $ABLH$ obtained during Summer 2016. Green, red and blue line represent $ABLH_{Ceilometer}$, $ABLH_{MWR}$ and $ABLH_{Doppler}$, respectively. The shadows represent the standard deviation of line with same color.

From this picture, we can observe the low variability of RL ($ABLH_{Ceilometer}$) and SBL ($ABLH_{MWR}$ and $ABLH_{Doppler}$) between 01:00 and 06:00 UTC. After this period the convective process increases, so that, the CBL ($ABLH_{MWR}$ and $ABLH_{Doppler}$) arises fastly, while the RL ($ABLH_{Ceilometer}$) ascends slowly. Approximately at 11:00 UTC the CBL breaks-up the RL and becomes full-developed. Consequently, all methods estimate the CBL height providing profiles with similar behaviors. After 16:00 UTC the difference between $ABLH_{Ceilometer}$ and other ones increase again because it returns to detect the RL other ones the SBL. The shadows (standard deviation) reinforce the similarity among the methods when the same sublayer is detected.

4. CONCLUSION

In this paper, we performed an estimation of $ABLH$ from three different tracers: w, θ, and vertical aerosol distribution, which were detected from Doppler lidar, MWR and Ceilometer data, respectively, during a campaign executed during Summer 2016 at IISTA-CEAMA. The $ABLH_{MWR}$ and $ABLH_{Doppler}$ present similar behavior during all periods, although the first one has a higher variability during the convective period. On the other hand the $ABLH_{Doppler}$ presents a high similarity with the other ABL heights only in the central region of the day. It occurs, because each method is based on a distinct $ABLH$ definition, consequently during the stable period, $ABLH_{MWR}$ and $ABLH_{Doppler}$ estimates the SBL height, while $ABLH_{Doppler}$. However, the joint observation of these three variables can provide a detailed comprehension about the sublayers that compound the ABL and how they interact along the time.

ACKNOWLEDGEMENTS

This work was supported by the Spanish Agencia Estatal de Investigación, AEI, through projects CGL2016-81092-R, CGL2017-83538-C3-1-R and CGL2017-90884-REDT. We acknowledge the financial support by the EU Horizon 2020 research and innovation program through project ACTRIS-2 (grant agreement No 654109) and, CNPQ by the Projects 152156/2018-6 and 432515/2018 and, Post-Doctor Scholarship (154320/2018-8).

REFERENCES

[1] Stull, R. B. An Introduction to Boundary Layer Meteorology. vol. 13, Kluwer Academic Publishers, the Netherlands, Dordrecht/Boston/London, 1988.
[2] Rose, T., Creewll, S., Löhnert, U., Simmer, C. A network suitable microwave radiometer for operational monitoring of cloudy atmosphere. Atmospheric Research, 75, 183 – 200 (2005).
[3] Navas-Guzmán, F., Fernández-Gálvez, J., Granados-Muñoz, M. J, Guerrero-Rascado, J. L., Bravo-Aranda, J. A., and Alados-Arboledas, L. Tropospheric water vapor and relative humidity profiles from lidar and microwave radiometry. Atmospheric Measurement Techniques, 7, 1201-1211 (2104).
[4] Holzworth, C. G. Estimates of mean maximum mixing depths in the contiguous United States. Monthly Weather Review, 92, 235–242 (1964).
[5] Stull, R. B. Meteorology for Scientists and Engineers. 3rd Edition, Uni. Of British Columbia, 2011.
[6] Moreira, G. A, Guerrero-Rascado, J. L., Bravo-Aranda, J. A., Benvant-Oltra, J. A., Ortiz-Amezcua, P., Róman, R., Bedoya-Velásquez, A. E., Landulfo, E., Alados-Arboledas, L., Sutdy of the planetary boundary layer by microwave radiometer, elastic lidar an Doppler lidar estimations in Southern Iberian Peninsula. Atmos Resear., 213, 185-195 (2018).
[7] Caicedo, V., Rappenglück, B., Lefer, B., Morris, G., Toledo, D., Delgado, R. Comparison of aerosol lidar retrieval methods for boundary layer height detection using ceilometer aerosol backscatter data. Atmospheric Measurement Techniques, 10, 1609–1622, (2017).